CLIMATOLOGY

Distinct impacts of major El Niño events on Arctic temperatures due to differences in eastern tropical Pacific sea surface temperatures

Hyein Jeong[1], Hyo-Seok Park[1,2]*, Malte F. Stuecker[3], Sang-Wook Yeh[1,2]

The El Niño Southern Oscillation (ENSO) is a climate mode in the tropical Pacific. The ENSO teleconnections are known to affect Arctic temperature; however, the robustness of this relationship remains debated. We find that Arctic surface temperatures during three major El Niño events are remarkably well simulated by a state-of-the-art model when nudged to the observed pantropical sea surface temperatures (SSTs). SST perturbation experiments show that the 1982–1983 warm pan-Arctic and the 1997–1998 cold pan-Arctic during winter can be explained by far eastern equatorial Pacific SSTs being higher during 1997–1998 than 1982–1983. Consistently, during the 2017–2018 La Niña, unusually low SSTs in the same region contributed to pan-Arctic warming. These pan-Arctic responses to the SSTs are realized through latent heating anomalies over the western and eastern tropical Pacific. These results highlight the importance of accurately representing SST amplitude and pattern for Arctic climate predictions.

INTRODUCTION

The strong Arctic secular warming trend in recent decades, particularly pronounced in late boreal autumn and winter, is superimposed by interannual variability. Much attention has been paid to this trend because of its crucial regional impacts and possible effects on the mid-latitude atmospheric circulation (1–3). In addition, Arctic warming in boreal winter can affect sea ice extent during the subsequent summer season (4–6). Whereas the Arctic warming trend is simulated by climate models (7, 8), the causes of interannual Arctic temperature fluctuations remain largely elusive. A prominent candidate is variations in tropical diabatic heating, which can be a key driver of the interannual and decadal variations of extratropical climate involving atmospheric teleconnections (9, 10).

In particular, the El Niño–Southern Oscillation (ENSO) has been suggested as a potentially important factor in Arctic climate variability (11–13). For instance, composites of reanalysis data indicate that El Niño events are usually accompanied by anomalous Arctic cooling and La Niña events by anomalous Arctic warming (12). However, a recent study found that the observed relationship between ENSO and Arctic surface temperature does not appear in historical climate model simulations, suggesting that the observed correlation could be an artifact associated with the internal variability of sea ice (14).

On interannual time scales, tropical sea surface temperature (SST) anomalies were most pronounced during three major El Niño events, 1982–1983, 1997–1998, and 2015–2016, providing an excellent testbed for elucidating how El Niño might affect Arctic climate. Despite their importance, there has been little modeling research on the tropics-to-Arctic teleconnection process during major El Niño events. So far, many previous studies attempted to illustrate the ENSO impact on Arctic climate under a linear framework, such as using

correlations between ENSO indices and Arctic temperatures (14, 15). However, a slight change in the zonal gradient of the eastern tropical Pacific convection during ENSO can lead to a very different extratropical teleconnection pattern, all the way up to the Arctic (16). Therefore, investigating similarities and differences between individual El Niño events and potential nonlinear effects might provide a better understanding of the tropics-to-Arctic teleconnection process.

Using a state-of-the-art ocean-atmosphere coupled climate model, we identify how major El Niño events and the accompanying pantropical SST anomalies affected Arctic climate. Specifically, this study presents new findings that each major El Niño event played a key role in observed Arctic winter temperatures and that slightly different SST patterns over the far eastern equatorial Pacific between these events caused markedly different Arctic temperature responses.

RESULTS

Observed climate conditions during major El Niño events

Major El Niño events are characterized by anomalously warm SSTs that peak in boreal winter in the eastern equatorial Pacific (around 160°E to 80°W). Figure 1 shows tropical SST anomalies averaged from December to March (DJFM) during 1982/1983 (Fig. 1A), 1997/1998 (Fig. 1B), and 2015/2016 (Fig. 1C) boreal winter. All events have eastern equatorial Pacific SST anomalies of more than 3°C and are accompanied by pronounced tropical Indian Ocean (IO) warming. While the eastern equatorial SST anomalies look similar to each other, there are distinct spatial SST patterns in the remaining tropics (fig. S1). At a closer look, there are also differences evident in the eastern equatorial Pacific. For instance, in 1982/1983 and 1997/1998, the eastern equatorial Pacific cold tongue was a lot warmer than usual, shifting the center of maximum SST anomalies toward the eastern side of the basin. These El Niño events are often referred to as Eastern Pacific (EP) El Niño (17–20). In contrast, the 2015/2016 El Niño event (Fig. 1C) is often classified as a "mixed type of El Niño," exhibiting both EP and central Pacific El Niño characteristics (21). The SST amplitude of the 2015/2016 El Niño event was very similar to those of the preceding two major El Niño events (22), but it decayed

[1]Institute of Ocean and Atmosphere Science (IOAS), Hanyang University, Ansan 15588, South Korea. [2]Department of Marine Science and Convergence Engineering, Hanyang University, Ansan 15588, South Korea. [3]Department of Oceanography and International Pacific Research Center, School of Ocean and Earth Science and Technology, University of Hawai'i at Mānoa, Honolulu, HI 96822, USA.
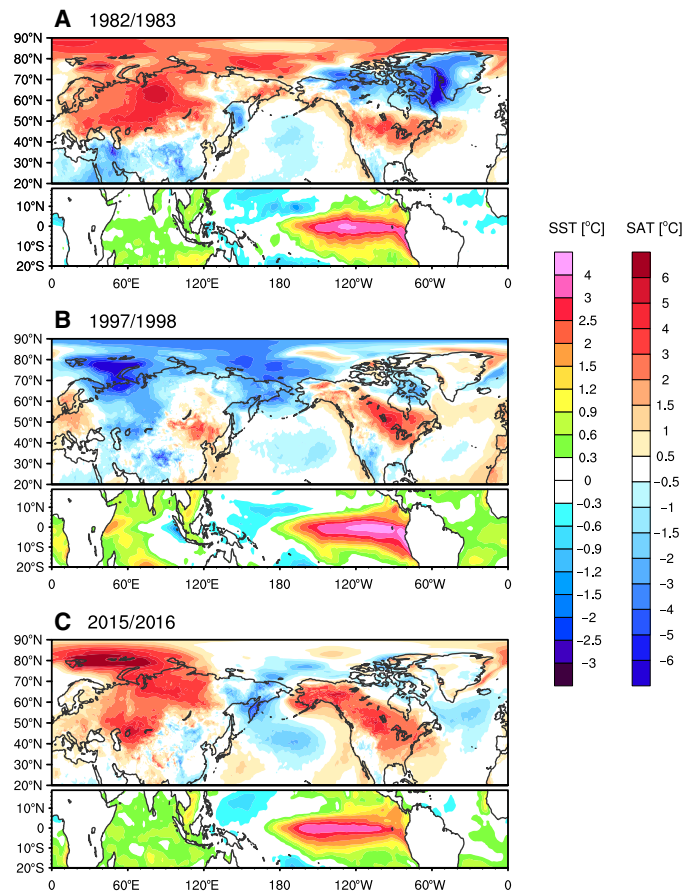*Corresponding author: Email: hspark1@gmail.com

Fig. 1. Observed tropical SST and extratropical surface air temperature anomalies during major El Niño events. Tropical (20°S to 20°N) SSTs (bottom; °C) and extratropical (20°N to 90°N) surface air temperature (SAT) (top; °C) anomalies during boreal winter (DJFM) of (**A**) 1982/1983, (**B**) 1997/1998, and (**C**) 2015/2016. SSTs and SAT are detrended and anomalies are relative to the 1982–2018 climatology.

a little earlier in winter (*23*). Therefore, the DJFM averaged warm SST anomalies in the equatorial Pacific are slightly smaller than those in 1982/1983 and 1997/1998.

El Niño events are usually accompanied by tropical IO warming (*24*). However, the IO warming patterns show some clear differences during the past three major El Niño events (*25*, *26*). While off-equatorial south IO warming occurred in 1982/1983 DJFM (Fig. 1A), a positive IO dipole mode pattern was seen in 1997/1998 DJFM (Fig. 1B) (*27*, *28*). A positive phase of the IO dipole mode refers to an SST pattern that features warm anomalies in the equatorial western IO and cold anomalies in the east (*27*). The IO dipole mode typically peaks in boreal autumn, but an anomalously strong event persisted throughout the winter of 1997/1998 (Fig. 1B). To investigate the Arctic response to not only the direct El Niño SST anomalies in the eastern equatorial Pacific but also associated pantropical SST anomalies (*29*), we impose pantropical SST anomalies in a coupled climate model for these three events (see Materials and Methods for details).

During major El Niño winters, a positive phase of the Pacific–North America (PNA) pattern is often seen (*30*), which is accompanied by cold surface temperature anomalies over the North Pacific and substantial warm anomalies over Canada and the northern United States during all three events (Fig. 1). Apart from these regions,

the northern extratropics had widely varying surface air temperature (SAT) anomalies during these three major El Niño winters. In particular, the Arctic and the Eurasian continent were a lot warmer than usual in the winter of 1982/1983 (Fig. 1A), whereas almost the opposite SAT anomalies were evident over the Arctic and the Eurasian continent in the winter of 1997/1998 (Fig. 1B) (*31*). In the winter of 2015/2016 El Niño, SAT anomalies over the Arctic and the Eurasian continent were higher than usual (Fig. 1C).

The relative importance of remote tropical forcing and atmospheric internal variability in the Arctic temperature variability remains strongly debated. Several studies (*14*, *32*) have argued that Arctic circulation changes and the accompanying temperature variability are mostly driven by internal variability in the historical and future CMIP5 (phase 5 of the Coupled Model Intercomparison Project) simulations. Specifically, a recent study (*14*) suggests that temperature variations over the Barents-Kara Sea are largely associated with the interaction between Arctic Sea ice cover and high-latitude atmospheric circulations rather than by ENSO-induced tropics-to-Arctic teleconnections. Provided that the Arctic SAT anomalies during the winters of 1982/1983 and 1997/1998, both of which were EP El Niño, show almost the opposite patterns (Fig. 1, A and B), internal atmospheric variability seems to play a key role for observed historical Arctic SAT variability. However, as will be shown later, we provide climate model evidence that part of the vastly different Arctic SAT anomalies seen during EP El Niño events can be explained by small but effective differences of the eastern equatorial Pacific SST anomalies during different events.

Model-simulated extratropical climate responses for major El Niño events

Changes in the diabatic heating field during El Niño are accompanied by large-scale divergence/convergence changes in the tropics (fig. S2), which can have pronounced remote impacts on global climate (*30*). Figure 2 shows the 200-hPa geopotential height (Z200) anomalies for the observations (left column) and the Community Earth System Model version 2 (CESM2) simulation ensemble mean (right column) for each El Niño event in the Northern Hemisphere during DJFM. Here, the anomalies in the CESM2 simulation are calculated as the differences between the El Niño pacemaker simulation and the control simulation. Throughout the manuscript, we consider the ensemble-mean (10 members for each experiment) response forced by tropical SST anomalies, whereas the ensemble spread is a measure of the unforced internal atmospheric variability in the model. The observed Z200 anomalies show a positive PNA-like pattern with a trough over the North Pacific and a ridge over North America for all three events (Fig. 2, A, C, and E). The model simulated ensemble-mean nonzonal Z200 patterns forced by tropical SST anomalies during each El Niño event are in good agreement with the observed Z200 characteristics, that is, a ridge over the tropical EP and the accompanying positive PNA-like pattern are well reproduced (Fig. 2, B, D, and F). The pattern correlation coefficients between the observed and CESM2 simulated nonzonal Z200 anomalies in the northern extratropics (30°N to 90°N) are 0.54, 0.75, and 0.35 for 1982/1983, 1997/1998, and 2015/2016, respectively. Except for 2015/2016, CESM2 forced by observed tropical SST reproduces well the extratropical teleconnection patterns. Following a recent study (*14*), we also carried out additional pacemaker simulations in the Niño3.4 region (10°S to 10°N, 160°E to 90°W) for the 1982/1983 and 1997/1998 El Niño events (fig. S3). In this case, the pattern
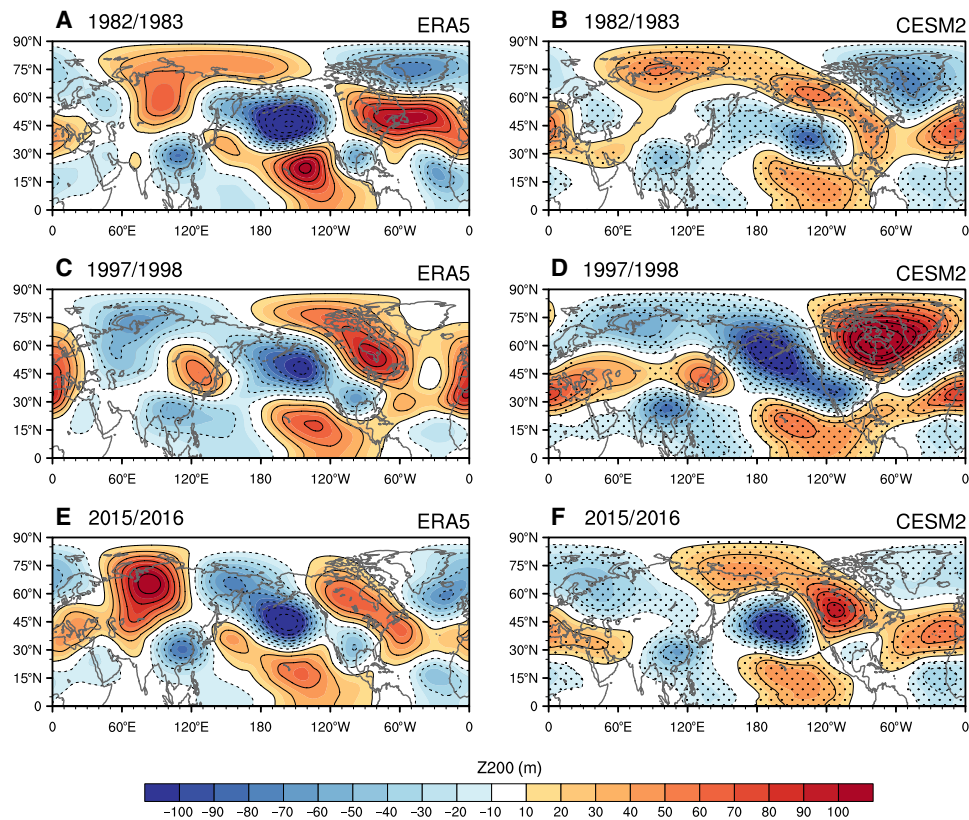
Fig. 2. Atmospheric teleconnection patterns during major El Niño events. Nonzonal component of 200-hPa geopotential height (in m) anomalies in the winter (DJFM) of (**A** and **B**) 1982/1983, (**C** and **D**) 1997/1998, and (**E** and **F**) 2015/2016, for the (A, C, and E) ERA5 reanalysis and (B, D, and F) CESM2 experiment ensemble mean. For the CESM2 experiment, statistically significant values ($P < 0.05$) are stippled.

correlations of nonzonal Z200 anomalies decrease from 0.54 to 0.43 for 1982/1983 and from 0.75 to 0.66 for 1997/1998. Thus, we conclude that nudging the entire tropical belt is necessary to obtain a more accurate simulation of tropics-to-extratropics teleconnections during ENSO.

While the mid-latitude nonzonal Z200 anomalies show positive PNA patterns with a notable ridge in the tropical EP for all the major El Niño events, the detailed Z200 anomalies at high latitudes are very different from each other. Although both the 1982/1983 and 1997/1998 El Niño events are regarded as EP El Niño events with strong warming over the eastern equatorial Pacific, Z200 over Greenland was anomalously low in the winter of 1982/1983 and anomalously high in 1997/1998 (Fig. 2, A and C). These contrasting responses are well captured by the CESM2 ensemble average (Fig. 2, B and D), indicating that the differing tropical SST pattern is the dominant cause instead of internal Arctic variability. Because the structure and strength of the El Niño–driven PNA pattern are somewhat sensitive to the longitudinal location and strength of tropical convection (*33*), small differences of eastern equatorial Pacific SSTs between 1982/1983 and 1997/1998 (fig. S1) might induce very different tropics-to-Arctic teleconnection patterns.

The Z200 anomalies in 2015/2016 winter (Fig. 2E) were similar to those in 1982/1983 (Fig. 2A) and are generally well simulated by the CESM2 ensemble mean (Fig. 2F), except for a strong ridge over western Russia that is evident in the observations but not in the ensemble-mean model response. The strong ridge over western

Russia during the winter of 2015/2016 could be due to atmospheric internal variability, which is unrelated to the tropical SST anomalies. We emphasize that climate models have some limitations in simulating the exact wintertime ENSO teleconnection patterns over the Northern Hemisphere extratropics (*34*).

Model-simulated Arctic SAT responses to major El Niño events
A polar stereographic view of the Arctic Ocean shows that a basin-wide Arctic Ocean surface warming (~3° to 3.5°C) occurred in the winter of 1982/1983 (Fig. 3A), whereas pronounced Arctic cold anomalies, almost the opposite to 1982/1983 and 2015/2016, occurred in 1997/1998 (Fig. 3B). The CESM2 ensemble-mean response reproduces the Arctic warm anomalies in 1982/1983 (Fig. 3D) and cold anomalies in 1997/1998 (Fig. 3E), suggesting that tropical heating was a key driver of Arctic SAT changes during these major El Niño events. Here, the mean response of 10 ensemble members is shown in Fig. 3 (D to F), for which most grid cells show statistically significant ($P < 0.05$) temperature anomalies (stippled). However, we emphasize that there are large SAT variations among the ensemble members, as expected from internal atmospheric variability. Figure 3G shows box plots for the Arctic Ocean–averaged ensemble-mean SAT anomalies simulated by CESM2, together with the ensemble spread. The interquartile SAT ranges are around 1.2° and 1.5°C in 1982/1983 and 1997/1998, respectively. The interquartile range is largest in 2015/2016, which is around 1.8°C. The observed Arctic Ocean
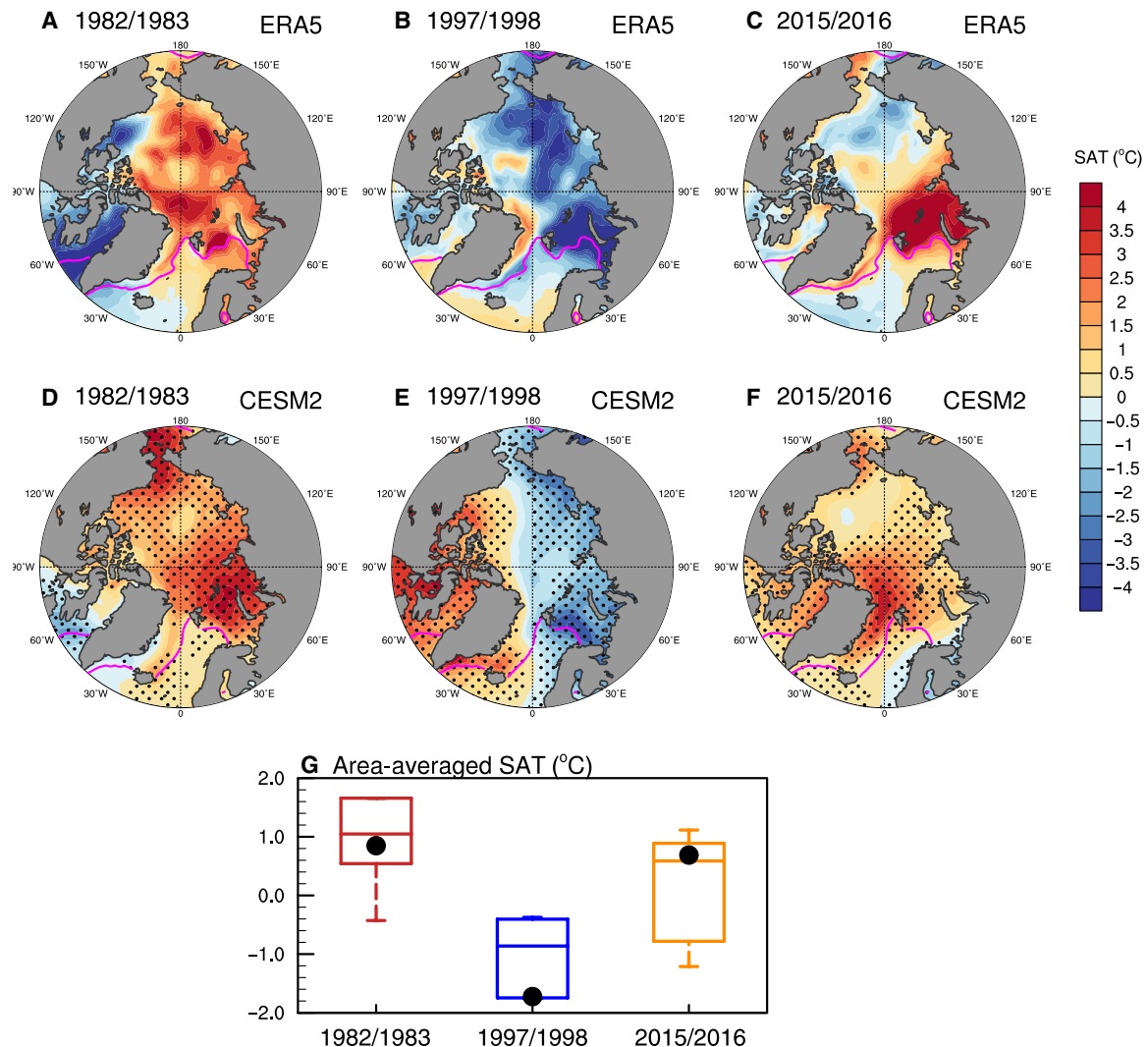
Fig. 3. Arctic Ocean surface temperature responses to major El Niño events. SAT (°C) anomalies in the Arctic Ocean averaged in the winter (DJFM) of (**A** and **D**) 1982/1983, (**B** and **E**) 1997/1998, and (**C** and **F**) 2015/2016 from (A to C) ERA5 reanalysis and (D to F) CESM2 simulation ensemble mean. For the CESM2 experiment, statistically significant values ($P < 0.05$) are stippled. Solid pink lines denote the climatological sea ice edges that correspond to 15% of sea ice concentration. (**G**) Box plots for ensemble mean and ensemble spread of CESM2-simulated SATs averaged over the Arctic Ocean (north of 60°N) in the winters of 1982/1983 (red), 1997/1998 (blue), and 2015/2016 (yellow). Shown in each box plot are the median (middle solid line), the 25th and 75th percentile (lower and upper hinge), and the 5th and 95th percentiles (whiskers) for the ensemble. The black dots indicate the SAT averaged over the Arctic Ocean for ERA5.

SAT anomalies fall within these model-simulated interquartile SAT ranges (black dots in Fig. 3G), although the CESM2-simulated Arctic SAT ensemble mean somewhat underestimates the cold anomalies during the winter of 1997/1998. In the winter of 2015/2016, SAT anomalies over the Barents-Kara seas were particularly high, up to 4°C higher than usual, whereas SAT over the Pacific sector of the Arctic was slightly lower than usual (Fig. 3C). CESM2 with tropical SST forcing does not simulate this strong warming over the Barents-Kara seas in the ensemble mean but simulates moderately strong warming over the Greenland seas (Fig. 3F).

The natural question arises of how the upper-level circulation anomalies regulate Arctic temperatures for these cases. Potential candidates are (i) dynamical warming or (ii) moisture transport and subsequent changes in downward longwave radiation. Previous studies have shown that Arctic surface warming can be caused by lower latitude forcing due to mid-tropospheric warming induced by anomalous poleward heat and moisture transport (*35*, *36*). Adiabatic warming is often suggested as a key linkage between mid-tropospheric warming and near-surface warming in the Arctic (*37*). Here, we calculate the lower-tropospheric heat budget for both the observations (fig. S4) and our CESM2 simulations (fig. S5), showing that the Arctic SAT anomaly pattern can be largely explained by increased downward longwave radiation. Horizontal temperature advection partly explains the SAT changes, especially the anomalously low SAT over the Pacific sector during the 1997/1998 El Niño (figs. S4 and S5). While it is difficult to rule out the role of adiabatic warming (*37*), lower tropospheric moisture flux into the Arctic was likely a key driver for the Arctic warming in 1982/1983 and cooling in 1997/1998.

Sensitivity of Arctic temperature to different tropical SST pattern

The almost opposite ensemble-mean response of Arctic Ocean surface temperatures between the winters of 1982/1983 (Fig. 3, A and D) and 1997/1998 (Fig. 3, B and E) indicates that there must be an important difference in the deep tropical SST pattern between 1982/1983 and 1997/1998. In this section, we attempt to find out the key tropical SST pattern causing this difference by performing several idealized perturbation experiments.

Role of tropical IO warming

The most notable feature of pantropical SSTs during the 1997/1998 El Niño, compared to 1982/1983, was an anomalously warm north IO

and a positive IO dipole pattern throughout the winter (Fig. 1B). To verify the impact of the tropical IO SST anomalies on Arctic temperatures during the winter of 1997/1998, we performed another idealized pacemaker experiment in which climatological SSTs were prescribed in the tropical IO, while other tropical SSTs in the other basins were restored to the observed SSTs. We can identify the impact of the tropical IO SST anomalies in 1997/1998 on extratropical climate by examining the ensemble-mean differences between the original experiment in which pantropical SSTs were prescribed (Fig. 4J) and this experiment in which tropical IO SSTs were prescribed as climatology (Fig. 4K). The difference of SSTs shows anomalously warm SSTs and the strengthening of diabatic heating over the tropical western IO (Fig. 4, L and I).
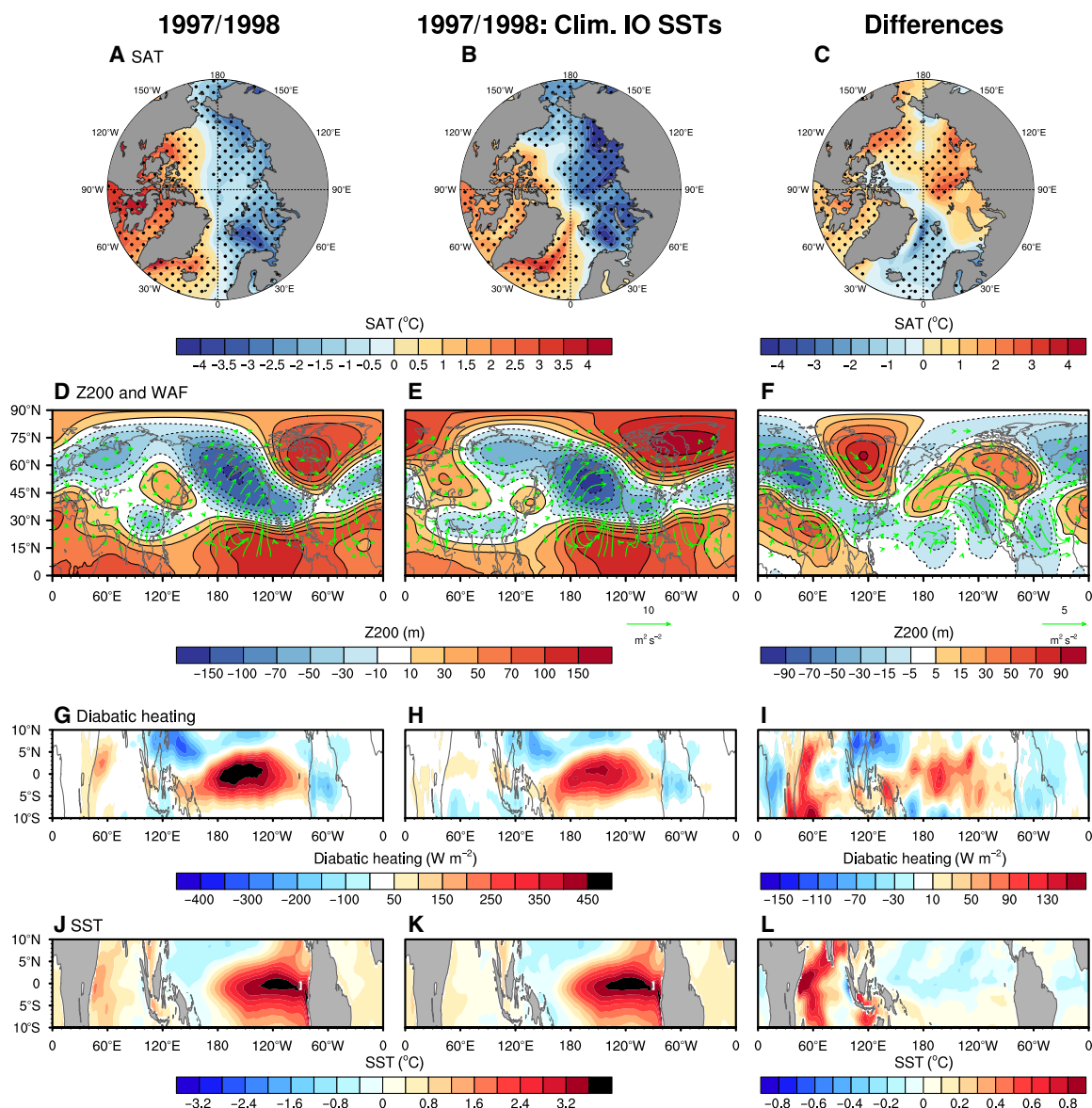

Fig. 4. Impacts of the tropical IO SST warming on the extratropics. (**A** to **C**) (Top) SAT anomalies over the Arctic Ocean, (**D** to **F**) (second row) 200-hPa geopotential height (shading; m) with wave activity flux (vector; $m^2 s^{-2}$) anomalies, (**G** to **I**) (third row) diabatic heating (W m^{-2}) integrated from 1000 to 200 hPa, and (**J** to **L**) (bottom) tropical SST anomalies in the winter (DJFM) of 1997/1998 for (A, D, G, and J) (left) the El Niño pacemaker simulation, (B, E, H, and K) (middle) cIO simulation, in which the climatological mean SSTs are restored to the tropical IO, and (C, F, I, and L) (right) differences between the El Niño pacemaker and the cIO experiments. Statistically significant values ($P < 0.05$) are stippled.

SAT over the Eurasian-Pacific sector of the Arctic decreases both in the pantropical SST forcing (Fig. 4A) and the tropical Pacific/Atlantic-only SST forcing (Fig. 4B). The difference between these experiments shows moderate warming in the eastern Arctic Ocean and the Beaufort Sea (Fig. 4C). This indicates that the western IO warming in 1997/1998 cannot serve as an explanation for the notable Arctic cold anomalies in 1997/1998 DJFM but instead likely contributed to mitigating the Arctic cold anomalies. Wave activity fluxes (38) show anomalously strong wave activity over the western IO and the subsequent north-eastward propagation of a wave train (Fig. 4F), which was a key factor for warming the eastern Arctic. This result is generally consistent with a recent study (39), which imposed a uniform 1°C SST warming in the tropical IO in a coupled climate model and found a moderate Arctic warming as a response. Note that the wave activity flux anomalies indicate not only a single wave train from the western IO to the eastern Arctic but also substantial changes in wave activities farther downstream, including the North Atlantic and Europe (Fig. 4F).

Role of far eastern equatorial Pacific warming

Another notable difference in tropical SSTs between the 1997/1998 and 1982/1983 El Niño events is that the equatorial Pacific SST anomaly in 1997/1998 El Niño was more oriented eastward, near South America (Fig. 1, A and B). Specifically, the maximum SST anomaly during the 1982/1983 El Niño was located around 135°W to 120°W, whereas the maximum SST anomaly during the 1997/1998 El Niño was located around 105°W (fig. S6). The SST difference between 1997/1998 and 1982/1983 shows that the far eastern equatorial Pacific was a lot warmer in 1997/1998 (fig. S1), which was accompanied by different diabatic heating fields in the tropics (fig. S2).

To identify the impact of the anomalously warm SSTs in the far equatorial EP during 1997/1998 on extratropical climate, we performed another idealized pacemaker experiment. Here, the anomalously warm SSTs in the far eastern equatorial Pacific were reduced (see Materials and Methods for details) so that the position of the maximum SST anomaly is shifted a little westward. By this method, the tropical SST anomalies in the winter of 1997/1998 (Fig. 5J) are modified to those seen in Fig. 5K (the difference between these two are presented in Fig. 5L).

The anomalously cold Arctic Ocean in the winter of 1997/1998 (Fig. 5A) changes to the anomalously warm Arctic Ocean in the reduced SST experiment (Fig. 5B). The difference of ensemble-mean SAT anomalies between these two simulations shows a pronounced cooling over almost the entire Arctic Ocean (Fig. 5C), indicating that the warm SST anomaly in the far eastern equatorial Pacific (Fig. 5L) is a key driver of the Arctic Ocean cooling. Z200 anomalies indicate that the positive PNA pattern shifts slightly eastward, leading to a weakening of the Aleutian Low and strengthening of the ridge over Greenland (Fig. 5F). Previous studies showed that shifting the maximum SST warm anomalies from the western Pacific to the EP can result in the PNA pattern shifting eastward (40–42). This study further shows that only modestly more SST warming in the far eastern equatorial Pacific (Fig. 5L) can cause a notable eastward shift of the PNA pattern (Fig. 5F).

Although the SST anomalies in the far eastern equatorial Pacific are relatively small between these two experiments, generally within 0.5°C, they have large influences on wave activity flux (Fig. 5F) and cause a ridge over Greenland, which can cause Arctic/Eurasian continent cooling (Fig. 5C). As warm SST anomalies expand further to the EP, diabatic heating also expands into the EP (Fig. 5I), leading to a more zonally elongated heating pattern (Fig. 5G). The 300-hPa stream function climatology and anomalies indicate that the 1997/1998 El Niño–induced extratropical wave anomalies are out of phase with the climatological stationary waves (fig. S7). This is generally consistent with previous studies (16, 43) showing that anomalously strong convective heating over the eastern equatorial Pacific destructively interferes with stationary waves, which can weaken poleward atmospheric energy transport (12, 16, 43).

So far, both the 1982/1983 and 1997/1998 El Niño events have been categorized as EP-type El Niño events. The present study, however, demonstrates that slightly more warming in the far eastern equatorial Pacific in 1997/1998 can cause a very different climate response in the northern extratropics including the Arctic, which might explain the observed extratropical SAT differences between these events (Fig. 1, A and B).

Potential Arctic temperature predictability resulting from the eastern equatorial Pacific SST pattern

If the far eastern equatorial Pacific warming during El Niño can cause pan-Arctic cooling, would the far eastern equatorial Pacific cooling during La Niña contribute to pan-Arctic warming? To answer this question, we examine two La Niña events in recent decades as case studies, specifically the winters of 2007/2008 and 2017/2018 (Fig. 6). 2007/2008 is recorded as one of the strongest La Niña winters since the satellite era. While both the 2007/2008 and 2017/2018 La Niña events are often classified as EP type of La Niña (18, 20), the regional-scale SST patterns show distinctions. The center of the negative SST anomalies was located at around 170°W in 2007/2008 (Fig. 6A), whereas the negative SST anomaly center in 2017/2018 was located at around 110°W, which is about 60° east of the 2007/2008 center.

The extratropical Z200 anomalies during these two La Niña winters are very different from each other. During the 2007/2008 winter, the Z200 anomalies in the Northern Hemisphere high latitudes are negative, projecting onto a positive Arctic Oscillation pattern (Fig. 6A). In contrast, during the 2017/2018 winter, the Z200 anomalies in the Northern Hemisphere high latitudes are positive, implying that the Arctic troposphere is warmer than usual. These contrasting responses are reproduced by our CESM2 experiments nudged to the observed pantropical SST (Fig. 6, C and D). The experiments also reproduce the anomalously high SAT in 2017/2018 over the Arctic Ocean (fig. S8), although the spatial pattern of the simulated Arctic SAT anomaly is somewhat different from the observations.

To further verify the effect of the far eastern equatorial cooling during the 2017/2018 La Niña on Arctic warming, we performed an additional idealized experiment. Here, the anomalously low SSTs in the far eastern equatorial Pacific (east of 120°W) were increased by 0.4°C (fig. S9). In this case, the simulated Z200 anomaly pattern in the Northern Hemisphere extratropics is very different from that of the original pacemaker simulation: The anomalously high Arctic Z200 in the original pacemaker simulation (Fig. 6D) flips into anomalous negative (fig. S9). In addition, the anomalously high Arctic SAT in the original pacemaker simulation changes into negative over the Pacific sector of the Arctic (fig. S9). These results support the hypothesis that the strong far EP cooling relative to the central Pacific cooling during 2017/2018 La Niña contributed to warming the pan-Arctic.
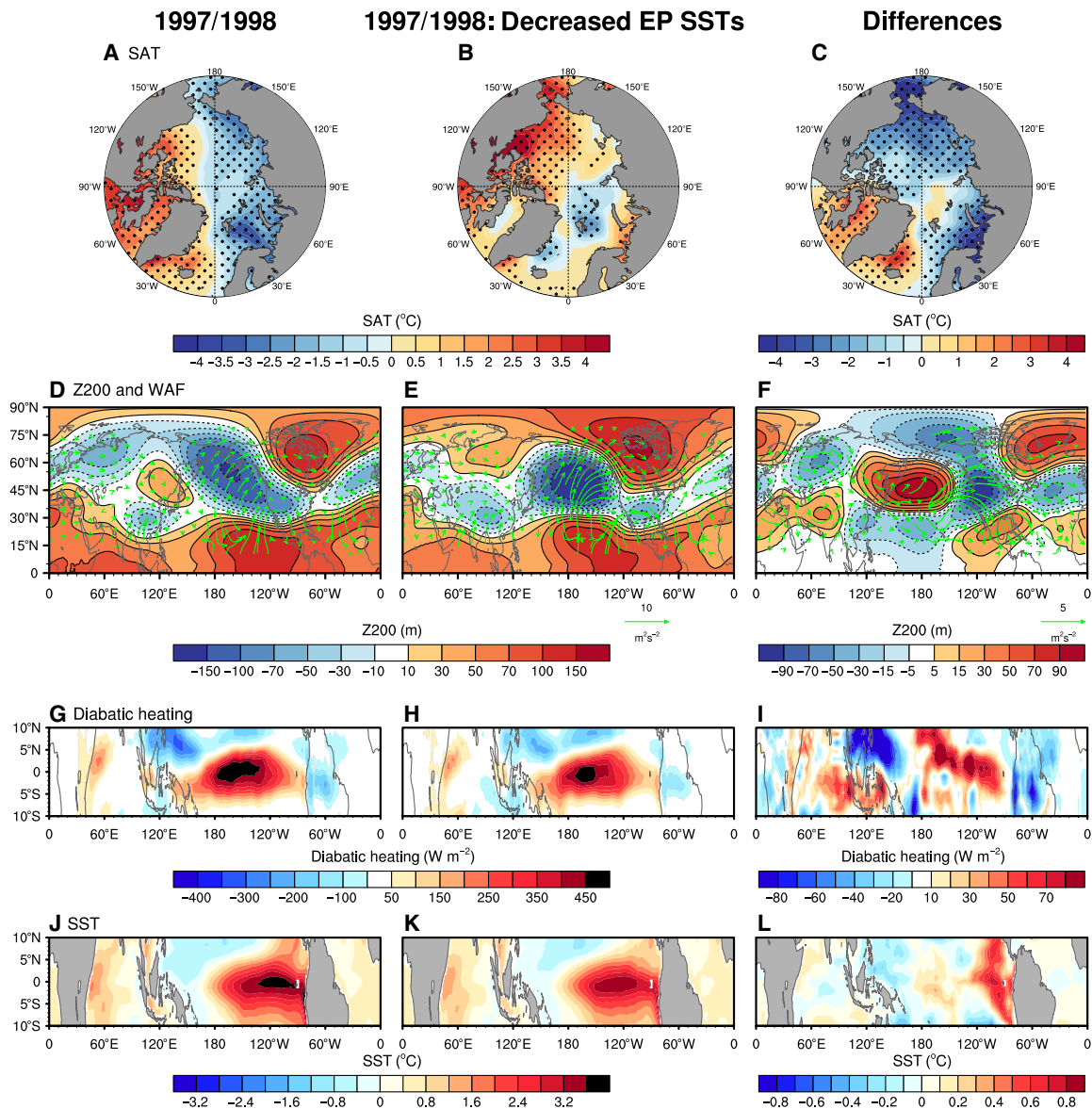
Fig. 5. Impacts of far eastern equatorial Pacific SST anomalies on the extratropics. (**A** to **C**) (Top) SAT anomalies over the Arctic Ocean, (**D** to **F**) (second row) 200-hPa geopotential height (shading; m) with wave activity flux (vector; m^2 s^{-2}) anomalies, (**G** to **I**) (third row) diabatic heating (W m^{-2}) integrated from 1000 to 200 hPa, and (**J** to **L**) (bottom) tropical SST anomalies in the winter (DJFM) of 1997/1998 for (A, D, G, and J) (left) the El Niño pacemaker simulation, (B, E, H, and K) (middle) dEP (decreased SST over the equatorial EP) simulation, in which the far equatorial EP SST anomalies are reduced, and (C, F, I, and L) (right) differences between the El Niño pacemaker and the dEP experiments. Statistically significant values ($P < 0.05$) are stippled.

DISCUSSION

In summary, our CESM2 pacemaker simulations demonstrate that wintertime Arctic temperature anomalies are strongly controlled by tropical SSTs during major El Niño events. In particular, the pronounced Arctic warming in the winter of 1982/1983 and cooling in 1997/1998 had large contributions from tropical SST anomalies. By performing additional model experiments, this study further shows that the anomalously high SSTs in the far eastern equatorial Pacific in the winter of 1997/1998 played a key role for the observed Arctic cooling by enhancing convective heating over the eastern tropical Pacific.

In the experiment in which the far eastern equatorial Pacific warming (near South America) in 1997/1998 was reduced, the simulated Arctic cooling is changed to Arctic warming, highlighting the extreme sensitivity of Arctic temperatures to the far eastern equatorial Pacific SSTs. So far, both the 1982/1983 and 1997/1998 El Niño have been categorized as EP El Niño, but this present study indicates that EP El Niño events need to be divided into "regular EP El Niño" and "far EP El Niño" events to better quantify their impacts on Arctic climate. Specifically, a far EP El Niño event can cause a ridge over Greenland and effectively decrease SAT over the Arctic and the Eurasian continent as shown in Fig. 5.
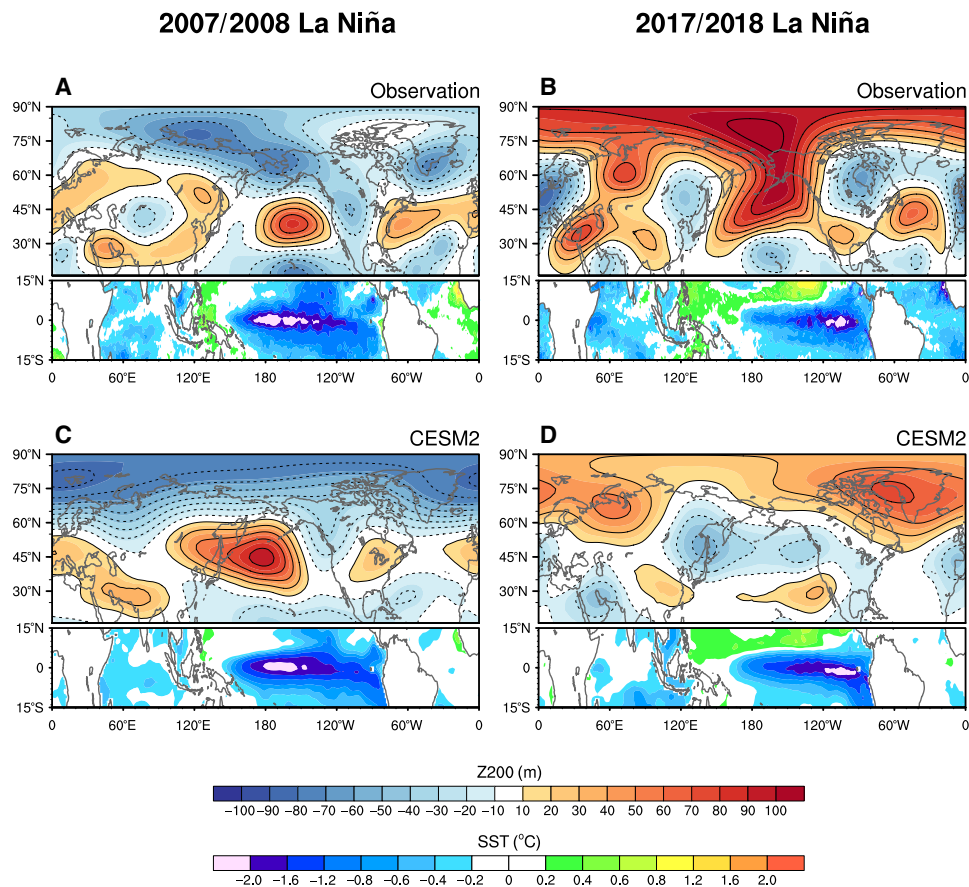
2007/2008 La Niña **2017/2018 La Niña**

Fig. 6. Impacts of tropical SST anomalies on the Northern Hemisphere extratropics during two La Niña events. (**A** and **B**) Observed and (**C** and **D**) CESM2-simulated, tropical (15°S to 15°N) SST (bottom; °C) and extratropical (15°N to 90°N) 200-hPa geopotential height anomalies (top; m) in the winter (DJFM) of (A and C) 2007/2008 and (B and D) 2017/2018.

This study has further shown that the eastern equatorial Pacific SST pattern also modulates the tropics-to-Arctic teleconnection during La Niña events. Our idealized model experiment shows that the relatively cold SST over the far eastern equatorial Pacific in 2017/2018 La Niña contributed to warming the pan-Arctic. These results suggest a largely linear relationship between the eastern equatorial Pacific SST pattern and the Arctic temperature such that the relatively warm eastern equatorial Pacific SST during El Niño can result in a relatively cold pan-Arctic, whereas relatively cold eastern equatorial Pacific SST during La Niña can result in a relatively warm pan-Arctic. This is generally consistent with existing theory (*12*) and further elucidates the key SST pattern that can explain how ENSO events can affect Arctic climate.

Our CESM2 simulations also suggest that tropical SST forcing may have a larger influence on Arctic SAT variability than previously thought. While numerous studies found dynamic linkages between tropical SST anomalies and the Arctic temperature and sea ice variability (*11–13, 37, 42*), a recent study questions the causality of the observed relationship between ENSO and Arctic surface temperature (*14*). This study indicates that if tropical SST anomalies are substantially large, as in these past three major El Niño events, the tropics-to-Arctic teleconnection can explain a large fraction of Arctic SAT variability. A potential caveat to note is that we only used

one model, thus not providing a quantification of structural model uncertainty. We believe that this finding provides a conceptual framework toward a better understanding of Arctic climate variability on interannual time scales.

MATERIALS AND METHODS
CESM2: Fully coupled model simulations
A fully coupled climate model, CESM2, was used to identify the role of major ENSO events in changing extratropical climate, especially the Arctic temperature during the boreal winter of 1982–1983, 1997–1998, 2007–2008, 2015–2016, and 2017–2018. The CESM2 consists of the atmosphere (CAM6; Community Atmosphere Model version 6) (*44*), ocean (POP2; Parallel Ocean Program version 2) (*45*), land (CLM5; Community Land Model version 5) (*46*), and sea ice (CICE5; Community Ice CodE version 5) (*47*) components. In this study, we used the "BHIST" compset, in which each component model is active. In the BHIST compset, historical emissions for anthropogenic and natural greenhouse gases are prescribed.

We used resolution "f09_g17" as a scientifically supported grid in CESM2. The atmospheric (CAM6) component uses a nominal 1° (1.25° in longitude and 0.9° in latitude) horizontal resolution with 32 vertical levels. The ocean (POP2) and sea ice (CICE5) component

models share the same horizontal resolution, which is nominal 1° with a uniform resolution of 1.125° in the zonal direction. The horizontal resolution in the meridional direction varies with the finest resolution of 0.27° at the equator. The ocean and sea ice components have 60 and 8 vertical levels, respectively. The frequency of the model output varies by variable. Most are saved as monthly averages, and a subset of variables is stored at intervals of 3-hourly, 6-hourly, or daily.

ENSO pacemaker simulations

We performed pacemaker ensemble simulations forced by tropical SST variability to identify the tropics-to-Arctic teleconnections for each major El Niño and La Niña event, by restoring the observed SSTs, from National Oceanic and Atmospheric Administration (NOAA) Optimum Interpolation Sea Surface Temperature (OISST) version 2 (48), in all three tropical ocean basins between 15°S and 15°N (fig. S10). The model-simulated tropical SSTs between 15°S and 15°N are restored to the observed SSTs by applying a 5-day relaxation time scale. For the 1982–1983 El Niño event, for example, the model-simulated tropical SSTs are restored to the observed tropical SSTs from April 1982 to March 1983. The simulation period for each El Niño and La Niña event is summarized in Table 1.

Following a recent study (14), we carried out additional pacemaker simulations, in which observed SSTs are nudged only over the Niño3.4 region (10°S to 10°N, 160°E to 90°W) (fig. S10) for the 1982–1983 and 1997–1998 El Niño events. Information for this additional pacemaker simulation is summarized in table S1.

Control simulations

For the control simulation, the tropical SSTs between 15°S and 15°N are restored to the observed climatological mean SSTs. Because of the increasing tropical SST trend, the climatological mean SSTs for the three El Niño and two La Niña events are defined differently: 1981–1999 average for 1982/1983 El Niño; 1986–2005 average for 1997/1998 El Niño; and 2000–2018 for 2007/2008 La Niña, 2015/2016 El Niño, and 2017–2018 La Niña events, respectively. These experiments are summarized in Table 1.

Idealized pacemaker experiments

To identify the tropical SST pattern contributing to the Arctic cooling in the winter of 1997/1998, two idealized perturbation experiments were performed. In addition, one idealized perturbation experiment was carried out for the Arctic warming in the winter of 2017/2018.

Climatological SST over the IO. To identify the impact of SST anomalies over the tropical IO on extratropical climate during the 1997/1998 DJFM, we conducted an idealized pacemaker simulation in which the model-simulated SSTs in the tropical IO were restored to the observed climatological mean SSTs. This "cIO" (climatological SST over the IO) experiment is the same as the pacemaker experiment for 1997/1998 except that the climatological mean SSTs are restored to the tropical IO.

Decreased SST over the equatorial EP. This experiment was designed to identify the impact of the far eastern equatorial Pacific SST warming on extratropical climate. In 1997/1998, the center of the equatorial Pacific SST anomalies is around 105°W (fig. S6). Here, the SST anomalies east of 105°W are replaced by the 1982/1983 SST anomalies. In addition, the positive SST anomalies from 120°E to 105°W were reduced by subtracting 50% of the SST difference between 1997/1998 and 1982/1983 from 120°E to 105°W. The resulting SST anomalies look like a mixture of 1997/1998 and 1982/1983 (fig. S6D): The center of the SST anomalies is 115°W, which is between the centers of 1982/1983 (128°W) and 1997/1998 (105°W). These two experiments are summarized in table S2.

Increased SST over the equatorial EP. This experiment was performed to identify the impact of the far eastern equatorial Pacific SST cooling on the Northern Hemisphere extratropical climate during the 2017/2018 winter. In 2017/2018, the center of the minimum equatorial Pacific SST anomaly is around 110°W (Fig. 6). Here, the SST anomaly east of 120°W is increased by 0.4°C so that the resulting SST anomaly has the pattern of a Central Pacific La Niña. Detailed information of this experiment is summarized in table S3.

Each simulation (experiment) has 10 ensemble members with different initial conditions. The anomalies are calculated from the differences between the El Niño pacemaker simulation and the control simulation.

Validation

The observed SST from the OISST (48) was used as references for comparison verification. For comparison of atmospheric fields, we used the latest climate reanalysis from the European Centre for Medium-Range Weather Forecasts (ECMWF) Reanalysis version 5 (ERA5) (49). To validate the simulated sea ice extent, we used the satellite-observed sea ice extent provided by the National Snow and Ice Data Center (NSIDC) (50). Throughout the manuscript, observed SSTs, SAT, and Z200 are detrended and then the anomalies are calculated by subtracting the long-term (1982–2018) climatological mean.

Statistical significance test

The standard bootstrap-based t test (51) was used for testing the statistical significance. The 10 ensemble member realizations of the Z200 and SAT variables from the two CESM2 pacemaker experiments are resampled randomly to construct 10,000 realizations for the population means and SDs. On the basis of the calculated t value from the population means and SDs, statistically significant values are calculated at the 95% confidence level.

Table 1. Time periods of CESM2 pacemaker simulations over pantropics. The three different periods for each El Niño pacemaker simulation and the corresponding averaging periods for calculating the climatological-mean SSTs.

Experiments	Target SST	1982/1983 El Niño	1997/1998 El Niño	2015/2016 El Niño	2007/2008 La Niña	2017/2018 La Niña
ENSO pacemaker simulations	Observed SSTs in the deep tropics	1982.04–1983.03	1997.04–1998.03	2015.04–2016.03	2007.04–2008.03	2017.04–2018.03
Control simulation	Climatological-mean SSTs in the deep tropics	Avg. (1981–1999)	Avg. (1986–2005)	Avg. (2000–2018)	Avg. (2000–2018)	Avg. (2000–2018)

Diabatic heating

To analyze the distribution of atmospheric convective heating associated with warm SST anomalies in the tropics, we calculated the total diabatic heating (Q) integrated from 1000 to 200 hPa, which is composed of radiation, latent heating, surface heat flux, and convergence of heat flux (52, 53)

$$Q = c_p \int_{P_2}^{P_1} \left(\frac{\partial T}{\partial t} - \omega \left(\frac{RT}{c_p p} - \frac{\partial T}{\partial p} \right) + \mathbf{V} \cdot \nabla T \right) \frac{dp}{g}$$

where c_p is the specific heat of dry air at constant pressure (1004.64 J K^{-1} kg^{-1}), P_1 and P_2 are 1000 and 200 hPa, respectively, T is the temperature, t is the time, ω is the vertical p velocity in units of Pa s^{-1}, R is the gas constant (287.04 J K^{-1} kg^{-1}), p is the pressure, $\mathbf{V}$ is the horizontal velocity vector, ∇ is the horizontal gradient operator, and g is the acceleration due to gravity (9.80665 ms^{-2}).

SUPPLEMENTARY MATERIALS

Supplementary material for this article is available at https://science.org/doi/10.1126/sciadv.abl8278

REFERENCES AND NOTES

1. J. A. Screen, C. Deser, D. M. Smith, X. Zhang, R. Blackport, P. J. Kushner, T. Oudar, K. E. McCusker, L. Sun, Consistency and discrepancy in the atmospheric response to Arctic sea-ice loss across climate models. *Nat. Geosci.* **11**, 155–163 (2018).
2. A. Dai, M. Song, Little influence of Arctic amplification on mid-latitude climate. *Nat. Clim. Chang.* **10**, 231–237 (2020).
3. J. Cohen, X. Zhang, J. Francis, T. Jung, R. Kwok, J. Overland, T. J. Ballinger, U. S. Bhatt, H. W. Chen, D. Coumou, S. Feldstein, H. Gu, D. Handorf, G. Henderson, M. Ionita, M. Kretschmer, F. Laliberte, S. Lee, H. W. Linderholm, W. Maslowski, Y. Peings, K. Pfeiffer, I. Rigor, T. Semmler, J. Stroeve, P. C. Taylor, S. Vavrus, T. Vihma, S. Wang, M. Wendisch, Y. Wu, J. Yoon, Divergent consensuses on Arctic amplification influence on midlatitude severe winter weather. *Nat. Clim. Chang.* **10**, 20–29 (2020).
4. H.-S. Park, S. Lee, Y. Kosaka, S.-W. Son, S.-W. Kim, The impact of Arctic winter infrared radiation on early summer sea ice. *J. Clim.* **28**, 6281–6296 (2015).
5. A. Letterly, J. Key, Y. Liu, The influence of winter cloud on summer sea ice in the Arctic, 1983–2013. *J. Geophys. Res.* **121**, 2178–2187 (2016).
6. B. M. Hegyi, P. C. Taylor, The unprecedented 2016–2017 Arctic sea ice growth season: The crucial role of atmospheric rivers and longwave fluxes. *Geophys. Res. Lett.* **45**, 5204–5212 (2018).
7. M. F. Stuecker, C. M. Bitz, K. C. Armour, C. Proistosescu, S. M. Kang, S.-P. Xie, D. Kim, S. M. Gregor, W. Zhang, S. Zhao, W. Cai, Y. Dong, F.-F. Jin, Polar amplification dominated by local forcing and feedbacks. *Nat. Clim. Chang.* **8**, 1076–1081 (2018).
8. H. Goosse, J. E. Kay, K. C. Armour, A. Bodas-Salcedo, H. Chepfer, D. Docquier, A. Jonko, P. J. Kushner, O. Lecomte, F. Massonnet, H.-S. Park, F. Pithan, G. Svensson, M. Vancoppenolle, Quantifying climate feedbacks in polar regions. *Nat. Commun.* **9**, 1919 (2018).
9. C. Stan, D. M. Straus, J. S. Frederiksen, H. Lin, E. D. Maloney, C. Schumacher, Review of tropical-extratropical teleconnections on intraseasonal time scales. *Rev. Geophys.* **55**, 902–937 (2017).
10. X. Yuan, M. R. Kaplan, M. A. Cane, The interconnected global climate system—A review of tropical–polar teleconnections. *J. Clim.* **31**, 5765–5792 (2018).
11. F. Sassi, D. Kinnison, B. A. Boville, R. R. Garcia, R. Roble, Effect of El Niño–Southern Oscillation on the dynamical, thermal, and chemical structure of the middle atmosphere. *J. Geophys. Res.* **109**, D17108 (2004).
12. S. Lee, Testing of the tropically excited Arctic warming mechanism (TEAM) with traditional El Niño and La Niña. *J. Clim.* **25**, 4015–4022 (2012).
13. C. Hu, S. Yang, Q. Wu, Z. Li, J. Chen, K. Deng, T. Zhang, C. Zhang, Shifting El Niño inhibits summer Arctic warming and Arctic sea-ice melting over the Canada Basin. *Nat. Commun.* **7**, 11721 (2016).
14. M. R. McCrystall, J. A. Screen, Arctic winter temperature variations correlated With ENSO are dependent on coincidental sea ice changes. *Geophys. Res. Lett.* **48**, e2020GL091519 (2021).
15. R. Clancy, C. Bitz, E. Blanchard-Wrigglesworth, The influence of ENSO on Arctic sea ice in large ensembles and observations. *J. Clim.* **34**, 9585–9604 (2021).
16. N. C. Johnson, Y. Kosaka, The impact of eastern equatorial Pacific convection on the diversity of boreal winter El Niño teleconnection patterns. *Clim. Dyn.* **47**, 3737–3765 (2016).
17. N. K. Larkin, D. E. Harrison, Global seasonal temperature and precipitation anomalies during El Niño autumn and winter. *Geophys. Res. Lett.* **32**, L16705 (2005).
18. J.-S. Kug, F.-F. Jin, S.-I. An, Two types of El Niño events: Cold tongue El Niño and warm pool El Niño. *J. Clim.* **22**, 1499–1515 (2009).
19. H. Y. Kao, J.-Y. Yu, Contrasting eastern-pacific and central-pacific types of ENSO. *J. Clim.* **22**, 615–632 (2009).
20. Z. Li, W. Zhang, M. F. Stuecker, H. Xu, F.-F. Jin, C. Liu, Different effects of two ENSO types on Arctic surface temperature in boreal winter. *J. Clim.* **32**, 4943–4961 (2019).
21. H. Paek, J.-Y. Yu, C. Qian, Why were the 2015/2016 and 1997/1998 extreme El Niños different? *Geophys. Res. Lett.* **44**, 1848–1856 (2017).
22. L. Chen, T. Li, B. Wang, L. Wang, Formation mechanism for 2015/16 super El Niño. *Sci. Rep.* **7**, 2975 (2017).
23. M. L. L'Heureux, K. Takahashi, A. B. Watkins, A. G. Barnston, E. J. Becker, T. E. Di Liberto, F. Gamble, J. Gottschalck, M. S. Halpert, B. Huang, K. Mosquera-Vásquez, A. T. Wittenberg, Observing and predicting the 2015/16 El Niño. *Bull. Am. Meteorol. Soc.* **98**, 1363–1382 (2017).
24. S. P. Xie, K. Hu, J. Hafner, H. Tokinaga, Y. Du, G. Huang, T. Sampe, Indian Ocean capacitor effect on Indo–western Pacific climate during the summer following El Niño. *J. Clim.* **22**, 730–747 (2009).
25. W. Zhang, Y. Wang, F.-F. Jin, M. F. Stuecker, A. G. Turner, Impact of different El Niño types on the El Niño/IOD relationship. *Geophys. Res. Lett.* **42**, 8570–8576 (2015).
26. S. Yang, Z. Li, J.-Y. Yu, X. Hu, W. Dong, S. He, El Niño-Southern Oscillation and its impact in the changing climate. *Natl. Sci. Rev.* **5**, 840–857 (2018).
27. N. H. Saji, B. N. Goswami, P. N. Vinayachandran, T. Yamagata, A dipole mode in the tropical Indian Ocean. *Nature* **401**, 360–363 (1999).
28. N. J. Abram, N. M. Wright, B. Ellis, B. C. Dixon, J. B. Wurtzel, M. H. England, C. C. Ummenhofer, B. Philibosian, S. Y. Cahyarini, T.-L. Yu, C.-C. Shen, H. Cheng, R. L. Edwards, D. Heslop, Coupling of Indo-Pacific climate variability over the last millennium. *Nature* **579**, 385–392 (2020).
29. M. F. Stuecker, C. M. Bitz, K. C. Armour, Conditions leading to the unprecedented low Antarctic sea ice extent during the 2016 austral spring season. *Geophys. Res. Lett.* **44**, 9008–9019 (2017).
30. S. W. Yeh, W. Cai, S. K. Min, M. J. McPhaden, D. Dommenget, B. Dewitte, M. Collins, K. Ashok, S. I. An, B. Y. Yim, J. S. Kug, ENSO atmospheric teleconnections and their response to greenhouse gas forcing. *Rev. Geophys.* **56**, 185–206 (2018).
31. J. C. Comiso, Warming trends in the Arctic from clear sky satellite observations. *J. Clim.* **16**, 3498–3510 (2003).
32. C. Deser, I. R. Simpson, K. A. McKinnon, A. S. Phillips, The Northern Hemisphere extratropical atmospheric circulation response to ENSO: How well do we know it and how do we evaluate models accordingly? *J. Clim.* **30**, 5059–5082 (2017).
33. N. Soulard, H. Lin, B. Yu, The changing relationship between ENSO and its extratropical response patterns. *Sci. Rep.* **9**, 6507 (2019).
34. R. Chen, I. R. Simpson, C. Deser, B. Wang, Model biases in the simulation of the springtime North Pacific ENSO teleconnection. *J. Clim.* **33**, 9985–10002 (2020).
35. K. Park, S. M. Kang, D. Kim, M. F. Stuecker, F. F. Jin, Contrasting local and remote impacts of surface heating on polar warming and amplification. *J. Clim.* **31**, 3155–3166 (2018).
36. S. He, X. Xu, T. Furevik, Y. Gao, Eurasian cooling linked to the vertical distribution of Arctic warming. *Geophys. Res. Lett.* **47**, e2020GL087212 (2020).
37. Q. Ding, J. M. Wallace, D. S. Battisti, E. J. Steig, A. J. Gallant, H. J. Kim, L. Geng, Tropical forcing of the recent rapid Arctic warming in northeastern Canada and Greenland. *Nature* **509**, 209–212 (2014).
38. R. A. Plumb, On the three-dimensional propagation of stationary waves. *J. Atmos. Sci.* **42**, 217–229 (1985).
39. S. Hu, A. V. Fedorov, Indian Ocean warming as a driver of the North Atlantic warming hole. *Nat. Commun.* **11**, 4785 (2020).
40. A. S. Taschetto, R. R. Rodrigues, G. A. Meehl, S. McGregor, M. H. England, How sensitive are the Pacific–tropical North Atlantic teleconnections to the position and intensity of El Niño-related warming? *Clim. Dyn.* **46**, 1841–1860 (2016).
41. Z. Q. Zhou, S. P. Xie, X. T. Zheng, Q. Liu, H. Wang, Global warming-induced changes in El Niño teleconnections over the North Pacific and North America. *J. Clim.* **27**, 9050–9064 (2014).
42. S. Matsumura, K. Yamazaki, T. Horinouchi, Robust asymmetry of the future Arctic polar vortex is driven by tropical Pacific warming. *Geophys. Res. Lett.* **48**, e2021GL093440 (2021).
43. M. Goss, S. B. Feldstein, S. Lee, Stationary wave interference and its relation to tropical convection and Arctic warming. *J. Clim.* **29**, 1369–1389 (2016).

44. V. E. Larson, CLUBB-SILHS: A parameterization of subgrid variability in the atmosphere. arXiv:1711.03675 [physics.ao-ph] (2017).

45. R. Smith, P. Jones, B. Briegleb, F. Bryan, G. Danabasoglu, J. Dennis, J. Dukowicz, C. Eden, B. Fox-Kemper, P. Gent, M. Hecht, "The Parallel Ocean Program (POP) reference manual: Ocean component of the Community Climate System Model (CCSM)" (Technical Report, Los Alamos National Laboratory, 2010).

46. D. M. Lawrence, R. A. Fisher, C. D. Koven, K. W. Oleson, S. C. Swenson, G. Bonan, N. Collier, B. Ghimire, L. van Kampenhout, D. Kennedy, E. Kluzek, P. J. Lawrence, F. Li, H. Li, D. Lombardozzi, W. J. Riley, W. J. Sacks, M. Shi, M. Vertenstein, W. R. Wieder, C. Xu, A. A. Ali, A. M. Badger, G. Bisht, M. van den Broeke, M. A. Brunke, S. P. Burns, J. Buzan, M. Clark, A. Craig, K. Dahlin, B. Drewniak, J. B. Fisher, M. Flanner, A. M. Fox, P. Gentine, F. Hoffman, G. Keppel-Aleks, R. Knox, S. Kumar, J. Lenaerts, L. R. Leung, W. H. Lipscomb, Y. Lu, A. Pandey, J. D. Pelletier, J. Perket, J. T. Randerson, D. M. Ricciuto, B. M. Sanderson, A. Slater, Z. M. Subin, J. Tang, R. Q. Thomas, M. V. Martin, X. Zeng, The community land model version 5: Description of new features, benchmarking, and impact of forcing uncertainty. J. Adv. Model. Earth Syst. 11, 4245–4287 (2019).

47. E. C. Hunke, W. H. Lipscomb, A. K. Turner, N. Jeffery, S. Elliott, "CICE: The Los Alamos Sea Ice Model Documentation and Software User's Manual Version 5.1" (Technical Report no. LA-CC-06-012, Los Alamos National Laboratory, 2015).

48. R. W. Reynolds, N. A. Rayner, T. M. Smith, D. C. Stokes, W. Wang, An improved in situ and satellite SST analysis for climate. J. Clim. 15, 1609–1625 (2002).

49. H. Hersbach, B. Bell, P. Berrisford, S. Hirahara, A. Horányi, J. Muñoz-Sabater, J. Nicolas, C. Peubey, R. Radu, D. Schepers, A. Simmons, C. Soci, S. Abdalla, X. Abellan, G. Balsamo, P. Bechtold, G. Biavati, J. Bidlot, M. Bonavita, G. De Chiara, P. Dahlgren, D. Dee, M. Diamantakis, R. Dragani, J. Flemming, R. Forbes, M. Fuentes, A. Geer, L. Haimberger, S. Healy, R. J. Hogan, E. Hólm, M. Janisková, S. Keeley, P. Laloyaux, P. Lopez, C. Lupu, G. Radnoti, P. de Rosnay, I. Rozum, F. Vamborg, S. Villaume, J.-N. Thépaut, The ERA5 global reanalysis. Q. J. R. Meteorol. Soc. 146, 1999–2049 (2020).

50. F. Fetterer, K. Knowles, W. N. Meier, M. Savoie, A. K. Windnagel, Sea ice index, version 3 (National Snow and Ice Data Center, 2017).

51. P. C. Austin, J. V. Tu, Bootstrap methods for developing predictive models. Am. Stat. 58, 131–137 (2004).

52. M. Yanai, S. Esbensen, J.-H. Chu, Determination of bulk properties of tropical cloud clusters from large-scale heat and moisture budgets. J. Atmos. Sci. 30, 611–627 (1973).

53. P. C. Hsu, T. Li, Interactions between boreal summer intraseasonal oscillations and synoptic-scale disturbances over the western North Pacific. Part II: Apparent heat and moisture sources and eddy momentum transport*. J. Clim. 24, 942–961 (2011).

54. S. Lee, T. Gong, N. Johnson, S. B. Feldstein, D. Pollard, On the possible link between tropical convection and the Northern Hemisphere Arctic surface air temperature change between 1958 and 2001. J. Clim. 24, 4350–4367 (2011).